

Neural Networks with Physics-Informed Architectures and Constraints for Dynamical Systems Modeling

Franck Djeumou ^{*1}, Cyrus Neary ^{*1}, Eric Goubault ², Sylvie Putot ², Ufuk Topcu ¹

¹ The University of Texas at Austin, United States

² LIX, CNRS, École Polytechnique, Institut Polytechnique de Paris, France

{fdjeumou, cneary, utopcu}@utexas.edu, {goubault, putot}@lix.polytechnique.fr

Abstract

Effective inclusion of physics-based knowledge into deep neural network models of dynamical systems can greatly improve data efficiency and generalization. Such a-priori knowledge might arise from physical principles (e.g., conservation laws) or from the system’s design (e.g., the Jacobian matrix of a robot), even if large portions of the system dynamics remain unknown. We develop a framework to learn dynamics models from trajectory data while incorporating a-priori system knowledge as inductive bias. More specifically, the proposed framework uses physics-based side information to inform the structure of the neural network itself, and to place constraints on the values of the outputs and the internal states of the model. It represents the system’s vector field as a composition of known and unknown functions, the latter of which are parametrized by neural networks. The physics-informed constraints are enforced via the augmented Lagrangian method during the model’s training. We experimentally demonstrate the benefits of the proposed approach on a variety of dynamical systems – including a benchmark suite of robotics environments featuring large state spaces, non-linear dynamics, external forces, contact forces, and control inputs. By exploiting a-priori system knowledge during training, the proposed approach learns to predict the system dynamics two orders of magnitude more accurately than a baseline approach that does not include prior knowledge, given the same training dataset.

Introduction

Owing to their tremendous capability to learn complex relationships from data, neural networks offer promise in their ability to model unknown dynamical systems from trajectory observations. Such models of system dynamics can then be used to synthesize control strategies, to perform model-based reinforcement learning, or to predict the future values of quantities of interest.

However, purely data-driven approaches to learning can result in poor data efficiency and in model predictions that violate physical principles. These deficiencies become particularly emphasized when the training dataset is relatively small – the neural network must learn to approximate a high-dimensional and non-linear map from a limited number of state trajectories. This limited reliability in the scarce data regime can render neural-network-based dynamics models impractical for the aforementioned applications.

^{*}These authors contributed equally.

On the other hand, useful a-priori system knowledge is often available, even in circumstances when the exact dynamics remain unknown. Such knowledge might stem from a variety of sources – basic principles of physics, geometry constraints arising from the system’s design, or empirically validated invariant sets in the state space. The central thesis of this paper is that effective inclusion of a-priori knowledge into the training of deep neural network models of dynamical systems can greatly improve data efficiency and model generalization to previously unseen regions of the state space, while also ensuring that the learned model respects physical principles.

We develop a framework to incorporate a wide variety of potential sources of a-priori knowledge into data-driven models of dynamical systems. The framework allows for arbitrary knowledge surrounding the functional form of the system’s vector field to be incorporated into the neural network structure, lending it more flexibility than a specific Lagrangian or Hamiltonian formulation of the dynamics, as has been considered in previous works. Furthermore, the framework is able to enforce physics-based constraints on the outputs and the internal states of the model, which is a novel capability in the context of neural network parametrizations of dynamical systems. These distinctions are discussed further in the section on related work below. We apply the proposed framework to a suite of high-dimensional and non-linear dynamical systems that include control inputs and contact forces. We are the first to consider such a suite of experiments in the context of physics-informed neural networks. The experiments demonstrate the viability of the proposed framework for the efficient learning of complex systems that are often used as challenging benchmark environments for deep reinforcement learning and model-based control (Duan et al. 2016; Freeman et al. 2021).

The proposed framework parametrizes the dynamical system’s vector field and uses numerical integration schemes to predict future states, as opposed to parametrizing a model that predicts the next state directly. This approach is similar to the neural ordinary differential equation (ODE) approach presented in (Chen et al. 2018), however, our proposed framework additionally incorporates physics-based knowledge as inductive bias in the model of the vector field. This incorporation of physics-based knowledge is accomplished via two distinct mechanisms:

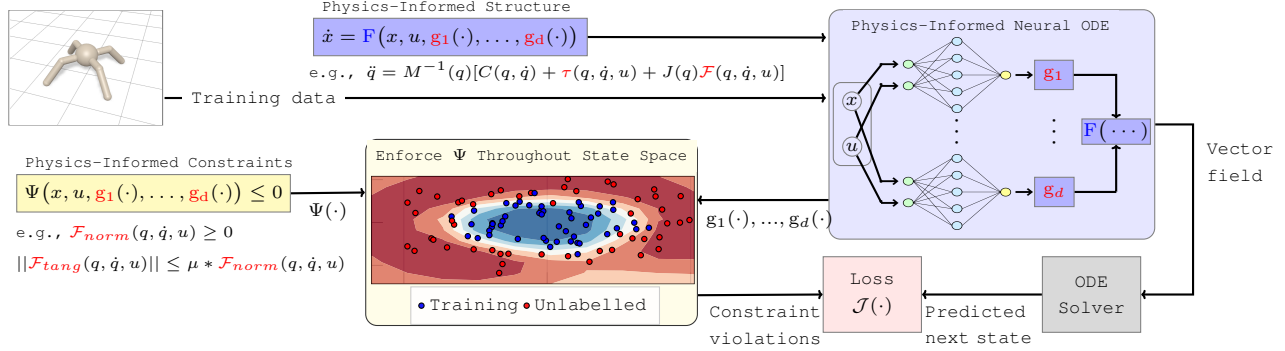


Figure 1: An illustration of the proposed framework. Training data in the form of sequences of (state, control input, next state) triplets are gathered from the system (*top left*). A-priori physics knowledge is captured by a structured representation of the vector field – unknown components are represented by neural networks (*blue*). Physics-based constraints are placed on the outputs of the model. These constraints are enforced not only on the labeled training datapoints, but also on any unlabeled points within the state space where the constraints are known to hold true (*yellow*).

1. Physics-informed model structure. We represent the system’s vector field as compositions of unknown terms that are parametrized as neural networks and known terms that are derived from a-priori knowledge. For example, Figure 1 illustrates a robotics environment in *Brax* (Freeman et al. 2021) whose equations of motion we assume to be partially known; the robot’s mass matrix is available, while the remaining terms in its equations of motion (i.e. its actuation and contact forces) must be learned. Neural networks representing the unknown terms are composed with the known mass matrix to obtain a model of the system’s vector field, as is illustrated in Figure 1. We discuss the general formulation of this compositional representation of the vector field below.

2. Physics-informed constraints. We additionally enforce physics-based constraints on the values of the outputs and the internal states of the model. Such constraints could, for example, encode known system equilibria, invariants, or symmetries in the dynamics.

We note that while only a limited number of datapoints may be available for supervised learning, constraints derived from a-priori knowledge will hold over entire subsets of the state space. In many cases, they will hold over the state space in its entirety. Ensuring that the learned model satisfies the relevant constraints throughout the state space, while also fitting the available trajectory data, leads to a semi-supervised learning scheme. The constraints are thus used to generalize the available training data to the unlabeled portions of the state space.

We train the model on time-series data of state and control input observations. The physics-informed model of the vector field is integrated in time to obtain predictions of the future state. These predictions are in turn compared against the true future state values obtained from training data to define the model’s loss. During the model’s training, we enforce the physics-informed constraints on a collection of points in the state space, both labeled and unlabeled, via the augmented Lagrangian method (Lu et al. 2021; Hestenes 1969).

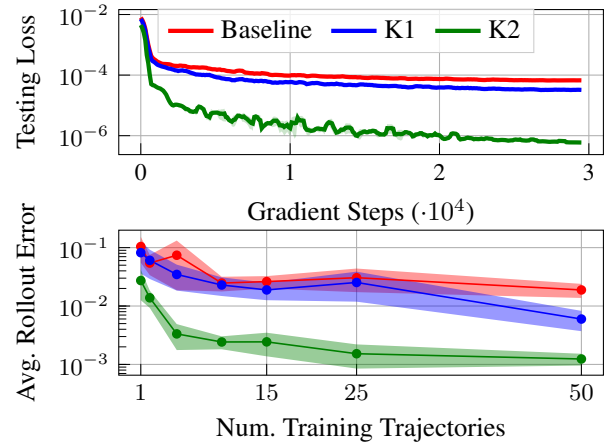


Figure 2: Incorporation of a-priori knowledge results in a significant improvement in data efficiency and out-of-sample prediction accuracy. *K1* stands for *knowledge 1* and corresponds to the incorporation of basic vector field knowledge: $\frac{dx}{dt} = v$. *K2* corresponds to knowledge of the mass matrix of the robot. The *Testing Loss* plot illustrates the model’s prediction errors during training. The *Avg. Rollout Error* plot illustrates a measure of the error over an entire predicted trajectory beginning from an out-of-sample initial state, after training has converged.

We experimentally demonstrate the effectiveness of the proposed approach on a suite of controlled rigid multi-body systems simulated in *Brax* (Freeman et al. 2021). We consider symmetries in the system vector fields, knowledge of the mass and Jacobian matrices of the robotic systems, and constraints that encode the laws of friction to help learn contact forces. We examine the extent to which these different sources of side information aid in improving the data efficiency and the out-of-sample prediction accuracy of the learned models. By exploiting a-priori system knowledge

during training, the proposed approach learns to predict system dynamics more than two orders of magnitude more accurately than a baseline approach that does not include any prior knowledge, as illustrated in Figure 2.

Related Work

Recent work has studied relationships between neural networks and differential equations (Lu et al. 2018; Dupont, Doucet, and Teh 2019; Kelly et al. 2020). In particular, (Chen et al. 2018) introduce the neural ODE; a neural network parametrization of ordinary differential equations. These works do not, however, consider how physics-based a-priori knowledge might be incorporated into the neural networks, which is the primary focus of this paper.

The inclusion of physics-based knowledge in the training of neural networks has, however, been studied extensively over the past several years. In particular, (Lu et al. 2021; Raissi, Perdikaris, and Karniadakis 2019; Raissi 2018; Han, Jentzen, and Weinan 2018; Sirignano and Spiliopoulos 2018; Long et al. 2018; Long, Lu, and Dong 2019) use neural networks for the solution and discovery of partial differential equations (PDE). However, our work focuses on using physics-based knowledge to instead model the vector field of dynamical systems.

More closely related to our work, a collection of recent papers also study how physics-based knowledge can be incorporated into neural networks for the learning of dynamics models from trajectory data (Zhong, Dey, and Chakraborty 2021; Hernández et al. 2021). Many of these works either use the Lagrangian or the Hamiltonian formulation of dynamics to inform the structure of a neural ODE, as in (Cranmer et al. 2020; Lutter, Ritter, and Peters 2019; Roehrl et al. 2020) vs. (Greydanus, Dzamba, and Yosinski 2019; Matsubara, Ishikawa, and Yaguchi 2020; Toth et al. 2020). A number of works (Zhong, Dey, and Chakraborty 2020b,a; Roehrl et al. 2020; Duong and Atanasov 2021; Gupta et al. 2020; Menda et al. 2019) have studied such Lagrangian or Hamiltonian neural networks in the context of learning control-oriented dynamics models. The authors of (Zhong and Leonard 2020; Allen-Blanchette et al. 2020) train Lagrangian neural networks using high-dimensional image and video data sources. We note however, that the majority of the above works employ a specific neural ODE structure that is dictated by the choice of either the Lagrangian or the Hamiltonian neural network formulation. This choice of a particular network structure renders them less flexible than the general framework for physics-informed neural networks that we propose. Furthermore, the examples explored in these works typically feature relatively low-dimensional state spaces that often do not include energy dissipation or external forces. By contrast, we apply the proposed approach to a variety of high-dimensional and complex systems. Finally, the above works do not consider the enforcement of physics-based constraints on the outputs and the internal states of the dynamics model.

Meanwhile, the authors of (Finzi, Wang, and Wilson 2020) explicitly enforce holonomic constraints on the state variables in Lagrangian and Hamiltonian neural networks.

This explicit constraint enforcement – accomplished via Lagrange multipliers – allows for the system dynamics to be expressed in Cartesian coordinates instead of generalized coordinates, simplifying the functional forms of the expressions that the neural networks must learn to fit. We note, however, that this method is restricted to equality constraints on state variables, and that the derivation of the solution to the Lagrange multiplier equations is only valid in the context of either Lagrangian or Hamiltonian neural networks. By contrast, we propose an approach that is independent of the selected physics-informed network structure and that is able to enforce inequality constraints on either the state variables or on the vector field itself.

A number of other recent works have also studied imposing constraints on the outputs of deep neural networks (Márquez-Neila, Salzmann, and Fua 2017; Fioretto et al. 2021). However, many of these works have different contexts and motivations than ours (Nandwani et al. 2019; Keradec et al. 2020). Most similar to our work are (Raissi, Perdikaris, and Karniadakis 2019; Dener et al. 2020), which both consider an augmented Lagrangian approach to the enforcement of physics-based constraints. However, the former focuses on PDE-constrained inverse design problems – the PDE is assumed to be known a-priori and is used to constrain a neural network parametrizing a solution to the differential equation. Meanwhile the latter uses constraints to enforce physical conservation properties while training a neural network to approximate the Focker-Planck collision operator used in fusion simulations.

Physics-Informed Neural Architectures

We consider arbitrary non-linear dynamics expressed in terms of the following ordinary differential equation (ODE):

$$\dot{x} = h(x, u). \quad (1)$$

The state $x : \mathbb{R}_+ \mapsto \mathcal{X}$ is a continuous-time signal, the control input $u : \mathbb{R}_+ \mapsto \mathcal{U}$ is a (possibly non-continuous) signal of time, and the vector field $h : \mathcal{X} \times \mathcal{U} \mapsto \mathbb{R}^n$ is assumed to be unknown and possibly non-linear. Here, n denotes the dimension of the state. We note that it is straightforward to explicitly include time dependency in (1), however, we omit it for clarity and notational simplicity.

Throughout the paper, we assume that a finite dataset \mathcal{D} of system trajectories – time-series data of states and control inputs – is available, in lieu of the system’s model. That is, we are given a set $\mathcal{D} = \{\tau_1, \dots, \tau_{|\mathcal{D}|}\}$ of trajectories $\tau = \{(x_0, u_0), (x_1, u_1), \dots, (x_T, u_T)\}$, where $x_i = x(t_i)$ is the state at time t_i , $u_i = u(t_i)$ is the control input applied at time t_i , and $t_0 < t_1 < \dots < t_T$ is an increasing sequence of points in time. We seek to learn a function to predict future state values $x_{k+1}, \dots, x_{k+n_r+1}$, given the current state value x_k and a sequence of control inputs u_k, \dots, u_{k+n_r} .

We propose to parameterize and to learn the unknown vector field h , as opposed to learning a prediction function that maps directly from a history of states and control inputs to the predicted next state. This choice to parametrize a model of the vector field is primarily motivated by the two following points: (1) A-priori knowledge derived from physical principles is typically most easily expressed in terms

of the system’s vector field; (2) Recent work (Chen et al. 2018) has demonstrated that parametrizing the vector field results in models that are able to approximate time-series data with more accuracy than approaches that directly estimate the next state. We thus build a framework capable of learning the vector field h from the dataset \mathcal{D} of trajectories, while also taking advantage of prior knowledge surrounding the functional form of the vector field.

Compositional Representation of the Vector Field. We represent the vector field of the dynamical system as the composition of a known function – derived from a-priori knowledge – and a collection of unknown functions that must be learned from data.

$$\dot{x} = h(x, u) = F(x, u, g_1(\cdot), \dots, g_d(\cdot)) \quad (2)$$

Here, F is a *known differentiable* function encoding available prior knowledge on the system’s model. The functions g_1, \dots, g_d encode the unknown terms within the underlying model. The inputs to these functions could themselves be arbitrary functions of the states and control inputs, or even of the outputs of the other unknown terms.

As an example, the reader can straightforwardly observe that such a model implicitly generalizes over the Lagrangian neural network formulation by considering the known part to be $F(q, \dot{q}, L) = (\nabla_{\dot{q}} \nabla_q^T L)^{-1} [\nabla_q L - (\nabla_{\dot{q}} \nabla_{\dot{q}}^T L) \dot{q}]$, where q and \dot{q} are the states of the system and $L(q, \dot{q})$ represents the unknown Lagrangian of the system.

End-To-End Training of the Model. Using the available training data, we learn the unknown functions $g_{\theta_1}, \dots, g_{\theta_d}$ in an end-to-end fashion. We parameterize g_1, \dots, g_d by a collection of neural networks $g_{\theta_1}, g_{\theta_2}, \dots, g_{\theta_d}$, where $\theta_1, \theta_2, \dots, \theta_d$ are the parameter vectors of each of the individual networks. For notational simplicity, we define $\Theta = (\theta_1, \dots, \theta_d)$ and we denote the collection of neural networks $g_{\theta_1}, g_{\theta_2}, \dots, g_{\theta_d}$ by G_Θ .

For fixed values of the parameters Θ , we integrate the current estimate of the dynamics $F(\cdot, \cdot, G_\Theta)$ using a differentiable ODE solver to obtain predictions of the future state. More specifically, given an increasing sequence of n_r distinct points in time $t_i < t_{i+1} < \dots < t_{i+n_r}$, an initial state x_i , and a sequence of control input values u_i, \dots, u_{i+n_r} , we use (3) to solve for the model-predicted sequence of future states $x_{i+1}^\Theta, \dots, x_{i+n_r+1}^\Theta$.

$$\begin{aligned} x_{i+1}^\Theta, \dots, x_{i+n_r+1}^\Theta = \\ \text{ODESolve}(x_k, u_i, \dots, u_{i+n_r}; F(\cdot, \cdot, G_\Theta)) \end{aligned} \quad (3)$$

The loss function $\mathcal{J}(\Theta)$ can then be constructed to minimize the state prediction error over the fixed rollout horizon n_r , as in (4).

$$\mathcal{J}(\Theta) = \sum_{\tau \in \mathcal{D}} \sum_{(x_i, u_i) \in \tau_l} \sum_{j=i}^{i+n_r} \|x_{j+1}^\Theta - x_{j+1}\|_2^2. \quad (4)$$

Finally, assuming that F is differentiable, we can update the weights in Θ by automatically differentiating through both ODESolve and the function F . We note that for each data-point (x_i, u_i) within each trajectory τ , we use the model to

roll out predictions of the next n_r states, which are in turn used to define the loss function. This use of rollouts instead of one-step predictions while defining the loss function results in better utilization of the available training data and in a reduction in error accumulation.

We note that the end-to-end training scheme described above is sensitive to the particular choice of integration scheme used in ODESolve. We consider such a choice to be a form of hyper-parameter tuning, which we discuss further in the supplementary material.

Physics-Informed Neural Network Constraints

In addition to using a-priori physics-based knowledge to dictate the structure of the neural network, we also use such knowledge to derive constraints on the outputs and the internal states of the model. More formally, suppose we derive a particular physics-informed model $F(x, u, G_\Theta)$ of the system’s vector field with unknown terms parametrized by the collection of neural networks G_Θ . Recall that $\Theta = (\theta_1, \theta_2, \dots, \theta_d)$ and that by G_Θ we denote $g_{\theta_1}, \dots, g_{\theta_d}$. Our objective is to solve for a set of parameter values minimizing the loss $\mathcal{J}(\Theta)$ over the training dataset while also satisfying all of the known physics-based constraints. That is, we aim to solve the optimization problem specified by (5)-(7).

$$\min_{\Theta} \mathcal{J}(\Theta) \quad (5)$$

$$\text{s.t. } \Phi_i(x, u, G_\Theta) = 0, \forall (x, u) \in \mathcal{C}_{\Phi_i}, i \in [v] \quad (6)$$

$$\Psi_j(x, u, G_\Theta) \leq 0, \forall (x, u) \in \mathcal{C}_{\Psi_j}, j \in [l] \quad (7)$$

Here, $\Phi_i(x, u, G_\Theta)$ and $\Psi_j(x, u, G_\Theta)$ are differentiable functions capturing the physics-informed equality and inequality constraints respectively. We use $[v] = \{1, \dots, v\}$ and $[l] = \{1, \dots, l\}$ to denote the sets indexing these constraints. For each constraint, we additionally assume there is some sub-set $\mathcal{C} \subseteq \mathcal{X} \times \mathcal{U}$, also derived from a-priori knowledge, over which the constraint should hold true. As elements $(x, u) \in \mathcal{C}$ are not necessarily included in the trajectory data used for training, the constraints thus provide useful information about potentially unlabeled points (x, u) that are not a part of the training dataset \mathcal{D} .

Enforcing Constraints Throughout the State Space. While (5)-(7) specifies that each constraint should hold over some known subset $\mathcal{C} \subseteq \mathcal{X} \times \mathcal{U}$, this formulation leads to a possibly infinite number of constraints. To solve the problem numerically, we instead select a finite set $\Omega = \{(x_1, u_1), (x_2, u_2), \dots, (x_{|\Omega|}, u_{|\Omega|})\} \subseteq \mathcal{X} \times \mathcal{U}$ of points throughout $\mathcal{X} \times \mathcal{U}$ at which we enforce the appropriate constraints. That is, we replace the possibly infinite sets of constraints given by (6)-(7) with the finite set of constraints given by (8)-(9).

$$\Phi_i(x, u, G_\Theta) = 0, \forall (x, u) \in \Omega \cap \mathcal{C}_{\Phi_i}, i \in [v] \quad (8)$$

$$\Psi_j(x, u, G_\Theta) \leq 0, \forall (x, u) \in \Omega \cap \mathcal{C}_{\Psi_j}, j \in [l] \quad (9)$$

Intuitively, by solving the optimization problem specified by (5), (8)-(9), we are finding the solution that fits the training data as well as possible, while also satisfying all of the relevant constraints at each point within a finite set Ω of representative states throughout $\mathcal{X} \times \mathcal{U}$.

Algorithm 1: Training Algorithm

Input: $F(\cdot)$, $\{\Phi_i(\cdot) | i \in [v]\}$, $\{\Psi_j(\cdot) | j \in [l]\}$, \mathcal{D} , Ω
Parameter: ϵ , μ , μ_{mult} , $N_{trainBatch}$, $N_{constrBatch}$
Output: Model parameters Θ .

- 1: Initialize model parameters Θ .
- 2: Initialize $\Lambda \leftarrow 0$; $\mu \leftarrow \mu_0$
- 3: **while** $(\sum_{i=1}^{N_\Phi} |\Phi_i| + \sum_{i=N_\Phi+1}^{|\Lambda|} \max\{0, \Psi_i\}) \geq \epsilon$ **do**
- 4: **while not** SGDStoppingCriterion() **do**
- 5: $\mathcal{D}_{batch} \leftarrow Sample(\mathcal{D}, N_{trainBatch})$
- 6: $\Omega_{batch} \leftarrow Sample(\Omega, N_{constrBatch})$
- 7: $\Theta \leftarrow optimUpdate(\mathcal{L}, \Theta, \mathcal{D}_{batch}, \Omega_{batch})$
- 8: **end while**
- 9: $\lambda_i \leftarrow \lambda_i + 2 * \mu * \Phi_i(x_i, u_i, G_\Theta), \forall i \in \{1, \dots, N_\Phi\}$
- 10: $\lambda_i \leftarrow \max\{0, \lambda_i + 2 * \mu * \Psi_i(x_i, u_i, G_\Theta)\}, \forall i \in \{N_\Phi + 1, \dots, |\Lambda|\}$
- 11: $\mu \leftarrow \mu * \mu_{mult}$
- 12: **end while**
- 13: **return** Θ

The Augmented Lagrangian Method. In order to solve this optimization problem, we propose to use a stochastic gradient descent (SGD) variant of the augmented Lagrangian method (Hestenes 1969). For each constraint defined in (8)-(9), we define a separate Lagrange variable $\lambda \geq 0$. That is, we define an individual variable λ for each equality constraint $\Phi_i, i \in [v]$ evaluated at each point $(x, u) \in \Omega \cap \mathcal{C}_{\Phi_i}$, and similarly for all of the inequality constraints Ψ_j . We note that there are at most $|\Omega|(v + l)$ such Lagrange variables to be defined.

Let $\Lambda = (\lambda_1, \lambda_2, \dots, \lambda_{|\Lambda|})$ denote the vector of all of the Lagrange variables. We define, for ease of presentation, an index $i \in \{1, 2, \dots, |\Lambda|\}$ that orders these variables λ_i along with their corresponding constraint functions and the points $(x_i, u_i) \in \Omega$ at which the constraint functions are evaluated. Without loss of generality, assume the first $\{1, \dots, N_\Phi\}$ indexes are assigned to Lagrange variables associated with equality constraints Φ , while the remaining $\{N_\Phi + 1, \dots, |\Lambda|\}$ indexes correspond to the inequality constraints Ψ . The augmented Lagrangian of the optimization problem (5), (8)-(9) is then given by (10).

$$\begin{aligned} \mathcal{L}(\Theta, \mu, \Lambda) = & \mathcal{J}(\Theta) + \mu \left[\sum_{i=1}^{N_\Phi} \Phi_i(x_i, u_i, G_\Theta)^2 \right. \\ & + \left. \sum_{i=N_\Phi+1}^{|\Lambda|} \max\{0, \Psi_i(x_i, u_i, G_\Theta)\}^2 \right] \\ & + \sum_{i=1}^{N_\Phi} \lambda_i \Phi_i(x_i, u_i, G_\Theta) + \sum_{i=N_\Phi+1}^{|\Lambda|} \lambda_i \Psi_i(x_i, u_i, G_\Theta) \end{aligned} \quad (10)$$

The Proposed Training Algorithm. Algorithm 1 outlines the proposed approach to solving optimization problem (5), (8)-(9). We initialize values for μ and Λ and minimize $\mathcal{L}(\Theta, \mu, \Lambda)$ via SGD over Θ while holding the values of μ and Λ fixed. To prevent the gradient descent from getting stuck in local minima, we randomly sample a subset of

points from Ω at each gradient update, instead of including the entire set in the definition of $\mathcal{L}(\Theta, \mu, \Lambda)$. This random selection of points at which to evaluate the constraint violations is akin to the random sampling of minibatches of training data during traditional SGD. Once this inner loop SGD has converged, we update the values of μ and Λ according to the update rules outlined in Algorithm 1. This process is repeated until the constraints are all satisfied, to within an allowed tolerance value ϵ .

Experimental Results

In this section we apply the proposed framework to a suite of controlled rigid multi-body systems simulated in Brax (Freeman et al. 2021). However, as an initial illustrative example of how the framework might be incorporate arbitrary a-priori within another context, we begin by numerically experimenting with the dynamics of a double pendulum.

Learning the Dynamics of a Double Pendulum

The dynamics of the double pendulum are described by (11).

$$\ddot{\phi}_1 = \frac{g_1 - \alpha_1 g_2}{1 - \alpha_1 \alpha_2}; \quad \ddot{\phi}_2 = \frac{-\alpha_2 g_1 + g_2}{1 - \alpha_1 \alpha_2} \quad (11)$$

Here, ϕ_1 and ϕ_2 specify the angular position of the first and second links of the pendulum, $\alpha_1(\phi_1, \phi_2) \propto \cos(\phi_1 - \phi_2)$, $\alpha_2(\phi_1, \phi_2) \propto \cos(\phi_2 - \phi_1)$, and $g_1(\phi_1, \phi_2, \dot{\phi}_1, \dot{\phi}_2)$, $g_2(\phi_1, \phi_2, \dot{\phi}_1, \dot{\phi}_2)$ are both complicated trigonometric functions of the state variables. We refer to the supplementary material for more details surrounding the dynamics.

By setting $x_1 = \phi_1$, $x_2 = \phi_2$, $x_3 = \dot{\phi}_1$, and $x_4 = \dot{\phi}_2$ we can thus express the dynamics as $\dot{x} = h(x)$, where $h_1(x) = x_3$, $h_2(x) = x_4$, and $h_3(x), h_4(x)$ are both given by (11).

Defining a Baseline for Comparison. As a baseline, we parametrize the vector field h by a single neural network g_{θ_1} . In terms of the framework outlined in the previous sections, we thus have $\Theta = \theta_1$ and $F(x, G_\Theta) = g_{\theta_1}(x)$.

(K1) Incorporating Knowledge of Equation (11). In order to demonstrate how arbitrary knowledge surrounding the system's vector field can be incorporated into the dynamics model, we assume that equation (11) is known, along with $\alpha_1(\cdot)$ and $\alpha_2(\cdot)$. However, we assume $g_1(\cdot)$ and $g_2(\cdot)$ are unknown. We parametrize g_1 and g_2 by two neural networks g_{θ_1} and g_{θ_2} , respectively. The proposed model for the vector field may thus be expressed as $F_1(x, G_\Theta) = x_3$, $F_2(x, G_\Theta) = x_4$, and with $F_3(x, G_\Theta), F_4(x, G_\Theta)$ both being functions of $\alpha_1, \alpha_2, g_{\theta_1}, g_{\theta_2}$, as in equation (11).

(K2) Incorporating Symmetry Constraints on g_1 and g_2 . To demonstrate that the proposed training algorithm properly enforces constraints on the system's dynamics, we impose equality constraints on $g_{\theta_1}, g_{\theta_2}$ derived from symmetries in the vector field. In particular, we impose four separate equality constraints, an example of which is as follows: $g_1(x_{1:2}, x_{3:4}) = -g_1(-x_{1:2}, x_{3:4})$. These equality constraints are enforced at a collection of points Ω that are sampled uniformly throughout the state space.

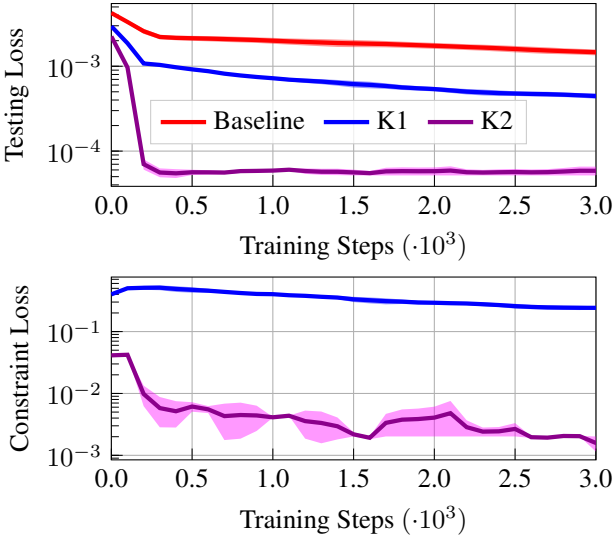


Figure 3: Numerical results for the double pendulum. The model is trained using a single trajectory consisting of 3 seconds worth of observation data.

Experimental Setup. Each neural network $g_{\theta_i}(x)$ is a multilayer perceptron (MLP) with ReLu activation functions and two hidden layers with 128 nodes each. We use a rollout horizon of $n_r = 5$ when defining the loss function and we randomly sample $|\Omega| = 10000$ points throughout the state space \mathcal{X} at which we enforce the above equality constraints. For further details on the setup of the experiment, we refer to the supplementary material.

Experimental Results. Figure 3 plots the results of training the various physics-informed models using only a single trajectory of data, which equivalent to 3 seconds worth of observations. We observe that in terms of prediction losses, (K1) performs better than the baseline, and (K2) performs better than both the baseline and (K1); its testing loss at convergence is roughly an order of magnitude lower than that of (K1). Furthermore, we observe that the constraint loss of (K2) – which measures the average value of the model’s violation of the equality constraints – is roughly two orders of magnitude lower than that of (K1). These results demonstrate the proposed framework’s effectiveness at incorporating a-priori system knowledge into the dynamics model. As more detailed knowledge is included into the model, the testing loss at convergence is significantly reduced. Furthermore, the gap in constraint loss between (K1) and (K2) demonstrates the effectiveness of the proposed framework in learning to fit the training data while simultaneously enforcing constraints on the vector field.

Learning the Dynamics of Controlled, Rigid, Multi-Body Systems

In this section we apply the proposed framework to a suite of robotic systems simulated in Brax (Freeman et al. 2021). These systems feature control inputs, non-linear dynamics, and external forces. Figure 4 illustrates the specific robotic

systems we use for testing.

The Governing Equations of Motion. The dynamics of all of the environments listed in Figure 4 can be described by the general equations of motion given in (12).

$$\ddot{q} = M(q)^{-1}[C(q, \dot{q}) + \tau(q, \dot{q}, u) + J(q)\mathcal{F}(q, \dot{q}, u)] \quad (12)$$

Here, q and \dot{q} represent the system state and its time derivative respectively, $M(q)$ represents the system’s mass matrix, $C(q, \dot{q})$ is a vector representing the Coriolis forces, $\tau(q, \dot{q}, u)$ is a vector representing the actuation forces (given the control input u), $J(q)$ is the system’s Jacobian matrix, and $\mathcal{F}(q, \dot{q}, u)$ is a vector representing the contact forces.

By setting $x_1 = q$ and $x_2 = \dot{q}$, we may re-write the system in the form of (1): $\dot{x} = h(x, u)$ where $h_1(x, u) = x_2$ and $h_2(x, u)$ is given by the right hand side of (12).

Defining a Baseline for Comparison. Similarly to the double pendulum baseline, we use a single neural network to parametrize the vector field, i.e. $F(x, u, G_{\Theta}) = g_{\theta_1}(x, u)$.

(K1) Incorporating Basic Knowledge on the Vector Field. A relatively simple piece of a-priori knowledge is that $\dot{x}_1 = x_2$. This follows directly from our formulation of the system’s dynamics, and it provides a useful piece of inductive bias surrounding the structure of the vector field. In our proposed framework, we again parametrize the vector field using a single neural network g_{θ_1} , however, we now have $F_1(x, u, G_{\Theta}) = x_2$ and $F_2(x, u, G_{\Theta}) = g_{\theta_1}(x, u)$.

(K2) Incorporating Knowledge of the Mass Matrix. We now assume the mass matrix $M(x_1)$ and the Coriolis force $C(x_1, x_2)$ terms are known a-priori. To use this a-priori knowledge, we parametrize the actuation force term and the contact force term using individual neural networks g_{θ_1} and g_{θ_2} . Our structured neural network model of the system dynamics may be written as follows: $F_1(x, u, G_{\Theta}) = x_2$ and $F_2(x, u, G_{\Theta}) = M^{-1}(x_1)C(x_1, x_2) + g_{\theta_1}(x, u) + g_{\theta_2}(x, u)$.

(K3) Incorporating Knowledge of the Jacobian Matrix. We assume, in addition to the a-priori knowledge assumed in (K3), that the system’s Jacobian matrix $J(x_1)$ is also known. Our structured neural network model can thus be written as $F_1(x, u, G_{\Theta}) = x_2$, $F_2(x, u, G_{\Theta}) = M^{-1}(x_1)C(x, x_2) + g_{\theta_1} + J(x_1)g_{\theta_2}$.

(K4) Incorporating Contact Force Constraints. We use the laws of friction to derive constraints on the contact forces between the robotic systems and the ground. In particular, we have $\mathcal{F}_{norm}(x, u) \leq 0$ and $\|\mathcal{F}_{tang}(x, u)\| \geq \mu\mathcal{F}_{norm}(x, u)$, where \mathcal{F}_{norm} represents the normal component of the contact forces and \mathcal{F}_{tang} is the tangential force vector. We assume (K4) has access to the same amount of a-priori knowledge as (K3), and that it additionally imposes the above inequality constraints on the neural network g_{θ_2} , which represents the contact force term.

Experimental Setup. We use the *Fetch* robot to compare the experimental results of the baseline, (K1), and (K2). We use the *Ant* robot to compare (K3) and (K4), examining the effect of including the contact force constraints.



Figure 4: Illustration of the suite of simulated robotic systems used during testing.

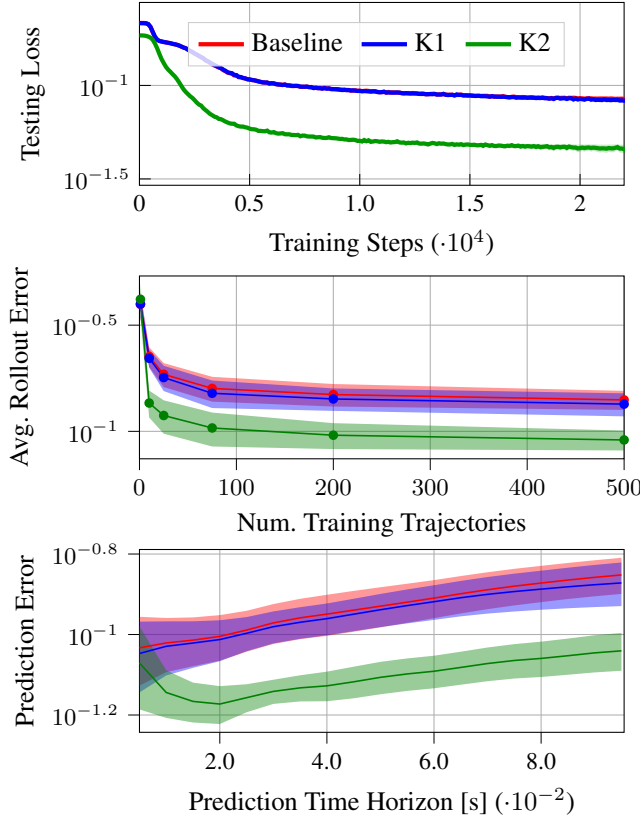


Figure 5: Numerical results for the *Fetch* robotic system.

The *Fetch* robot has a 143-dimensional state space and a 10-dimensional control input space. Meanwhile, the *Ant* robot has a 117-dimensional state space and an 8-dimensional action space. To parametrize each unknown term g_{θ_i} we use a multilayer perceptron (MLP) with ReLu activation functions and two hidden layers of 256 nodes each. We use a rollout horizon of $n_r = 5$ to define the loss function, as described in (4). Further details are given in the supplementary material.

Experimental Results. Figure 5 illustrates the results of training the baseline, $(K1)$, and $(K2)$ on the *Fetch* robot. Figure 6 compares the extents to which $(K3)$ and $(K4)$ violate the contact force constraints on the *Ant* robot. Similarly to the double pendulum study, we observe from Figure 5 that as we increase the amount of a-priori knowledge incorporated into the model, the average prediction error correspondingly decreases. In particular, the *Avg. Rollout Error*

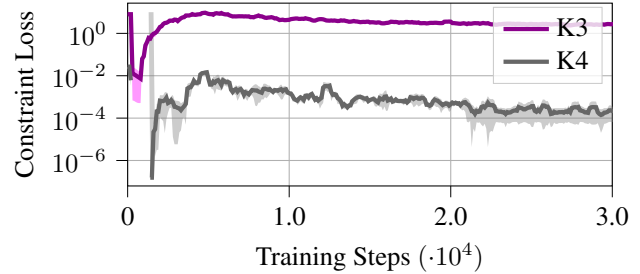


Figure 6: Constraint loss for the *Ant* robotic system. The plotted values measure the extent at which the learned models violate the constraints on the values of the contact forces between the robot and the ground.

plot shows that by incorporating a-priori knowledge of the mass matrix, $(K2)$ consistently makes more accurate predictions than either the baseline or $(K1)$, regardless of the number of trajectories included in the training dataset. From Figure 6, we observe a gap of four orders of magnitude between the constraint loss of $(K3)$ and $(K4)$: the proposed algorithm learns a model that effectively enforces the contact force constraints incorporated into $(K4)$.

Conclusions

In this work we present a framework for the incorporation of a-priori physics-based knowledge into neural network models of dynamical systems. We present a suite of numerical experiments that exemplify the effectiveness of the proposed approach: the inclusion of increasingly detailed forms of side-information leads to increasingly accurate model predictions. We also demonstrate that the framework effectively enforces physics-based constraints on the outputs and internal states of the models. Future work will aim to use these physics-informed dynamics models for control.

References

- Allen-Blanchette, C.; Veer, S.; Majumdar, A.; and Leonard, N. E. 2020. LagNetViP: A Lagrangian Neural Network for Video Prediction. arXiv:2010.12932.
- Assencio, D. 2014. The double pendulum: Lagrangian formulation. <https://diego.assencio.com/?index=1500c66ae7ab27bb0106467c68feebc6>. Accessed: 2021-09-08.
- Bradbury, J.; Frostig, R.; Hawkins, P.; Johnson, M. J.; Leary, C.; Maclaurin, D.; Necula, G.; Paszke, A.; VanderPlas, J.;

Wanderman-Milne, S.; and Zhang, Q. 2018. JAX: composable transformations of Python+NumPy programs.

Chen, R. T.; Rubanova, Y.; Bettencourt, J.; and Duvenaud, D. 2018. Neural ordinary differential equations. In *Proceedings of the 32nd International Conference on Neural Information Processing Systems*, 6572–6583.

Cranmer, M.; Greydanus, S.; Hoyer, S.; Battaglia, P.; Spergel, D.; and Ho, S. 2020. Lagrangian Neural Networks. arXiv:2003.04630.

Dener, A.; Miller, M. A.; Churchill, R. M.; Munson, T.; and Chang, C.-S. 2020. Training neural networks under physical constraints using a stochastic augmented Lagrangian approach. arXiv:2009.07330.

Dormand, J. R.; and Prince, P. J. 1980. A family of embedded Runge-Kutta formulae. *Journal of computational and applied mathematics*, 6(1): 19–26.

Duan, Y.; Chen, X.; Houthooft, R.; Schulman, J.; and Abbeel, P. 2016. Benchmarking deep reinforcement learning for continuous control. In *International conference on machine learning*, 1329–1338. PMLR.

Duong, T.; and Atanasov, N. 2021. Hamiltonian-based Neural ODE Networks on the SE (3) Manifold For Dynamics Learning and Control. In *Robotics: Science and Systems (RSS)*.

Dupont, E.; Doucet, A.; and Teh, Y. W. 2019. Augmented neural ODEs. In *Proceedings of the 33rd International Conference on Neural Information Processing Systems*, 3140–3150.

Finzi, M.; Wang, K. A.; and Wilson, A. G. 2020. Simplifying Hamiltonian and Lagrangian Neural Networks via Explicit Constraints. In Larochelle, H.; Ranzato, M.; Hadsell, R.; Balcan, M. F.; and Lin, H., eds., *Advances in Neural Information Processing Systems*, volume 33, 13880–13889. Curran Associates, Inc.

Fiorotto, F.; Van Hentenryck, P.; Mak, T. W. K.; Tran, C.; Baldo, F.; and Lombardi, M. 2021. Lagrangian Duality for Constrained Deep Learning. In Dong, Y.; Ifrim, G.; Mladenić, D.; Saunders, C.; and Van Hoecke, S., eds., *Machine Learning and Knowledge Discovery in Databases. Applied Data Science and Demo Track*, 118–135. Cham: Springer International Publishing. ISBN 978-3-030-67670-4.

Freeman, C. D.; Frey, E.; Raichuk, A.; Girgin, S.; Mordatch, I.; and Bachem, O. 2021. Brax – A Differentiable Physics Engine for Large Scale Rigid Body Simulation. arXiv:2106.13281.

Greydanus, S.; Dzamba, M.; and Yosinski, J. 2019. Hamiltonian neural networks. *Advances in Neural Information Processing Systems*, 32: 15379–15389.

Gupta, J. K.; Menda, K.; Manchester, Z.; and Kochenderfer, M. 2020. Structured mechanical models for robot learning and control. In *Learning for Dynamics and Control*, 328–337. PMLR.

Han, J.; Jentzen, A.; and Weinan, E. 2018. Solving high-dimensional partial differential equations using deep learning. *Proceedings of the National Academy of Sciences*, 115(34): 8505–8510.

Hernández, Q.; Badías, A.; González, D.; Chinesta, F.; and Cueto, E. 2021. Structure-preserving neural networks. *Journal of Computational Physics*, 426: 109950.

Hestenes, M. R. 1969. Multiplier and gradient methods. *Journal of optimization theory and applications*, 4(5): 303–320.

Kelly, J.; Bettencourt, J.; Johnson, M. J.; and Duvenaud, D. K. 2020. Learning Differential Equations that are Easy to Solve. In Larochelle, H.; Ranzato, M.; Hadsell, R.; Balcan, M. F.; and Lin, H., eds., *Advances in Neural Information Processing Systems*, volume 33, 4370–4380. Curran Associates, Inc.

Kervadec, H.; Dolz, J.; Yuan, J.; Desrosiers, C.; Granger, E.; and Ayed, I. B. 2020. Constrained Deep Networks: Lagrangian Optimization via Log-Barrier Extensions. arXiv:1904.04205.

Long, Z.; Lu, Y.; and Dong, B. 2019. PDE-Net 2.0: Learning PDEs from data with a numeric-symbolic hybrid deep network. *Journal of Computational Physics*, 399: 108925.

Long, Z.; Lu, Y.; Ma, X.; and Dong, B. 2018. Pde-net: Learning pdes from data. In *International Conference on Machine Learning*, 3208–3216. PMLR.

Lu, L.; Pestourie, R.; Yao, W.; Wang, Z.; Verdugo, F.; and Johnson, S. G. 2021. Physics-informed neural networks with hard constraints for inverse design. arXiv:2102.04626.

Lu, Y.; Zhong, A.; Li, Q.; and Dong, B. 2018. Beyond finite layer neural networks: Bridging deep architectures and numerical differential equations. In *International Conference on Machine Learning*, 3276–3285. PMLR.

Lutter, M.; Ritter, C.; and Peters, J. 2019. Deep Lagrangian Networks: Using Physics as Model Prior for Deep Learning. arXiv:1907.04490.

Matsubara, T.; Ishikawa, A.; and Yaguchi, T. 2020. Deep Energy-based Modeling of Discrete-Time Physics. In Larochelle, H.; Ranzato, M.; Hadsell, R.; Balcan, M. F.; and Lin, H., eds., *Advances in Neural Information Processing Systems*, volume 33, 13100–13111. Curran Associates, Inc.

Menda, K.; Gupta, J. K.; Manchester, Z.; and Kochenderfer, M. J. 2019. Structured Mechanical Models for Efficient Reinforcement Learning. In *Workshop on Structure and Priors in Reinforcement Learning, International Conference on Learning Representations (ICLR)*, 138–171.

Márquez-Neila, P.; Salzmann, M.; and Fua, P. 2017. Imposing Hard Constraints on Deep Networks: Promises and Limitations. arXiv:1706.02025.

Nandwani, Y.; Pathak, A.; Singla, P.; et al. 2019. A primal dual formulation for deep learning with constraints. In *Advances in Neural Information Processing Systems*, 12157–12168.

Raissi, M. 2018. Deep hidden physics models: Deep learning of nonlinear partial differential equations. *The Journal of Machine Learning Research*, 19(1): 932–955.

Raissi, M.; Perdikaris, P.; and Karniadakis, G. E. 2019. Physics-informed neural networks: A deep learning framework for solving forward and inverse problems involving nonlinear partial differential equations. *Journal of Computational Physics*, 378: 686–707.

Roehrl, M. A.; Runkler, T. A.; Brandstetter, V.; Tokic, M.; and Obermayer, S. 2020. Modeling system dynamics with physics-informed neural networks based on lagrangian mechanics. *IFAC-PapersOnLine*, 53(2): 9195–9200.

Sirignano, J.; and Spiliopoulos, K. 2018. DGM: A deep learning algorithm for solving partial differential equations. *Journal of computational physics*, 375: 1339–1364.

Toth, P.; Rezende, D. J.; Jaegle, A.; Racanière, S.; Botev, A.; and Higgins, I. 2020. Hamiltonian Generative Networks. In *8th International Conference on Learning Representations, ICLR 2020, Addis Ababa, Ethiopia, April 26-30, 2020*. OpenReview.net.

Zhong, Y. D.; Dey, B.; and Chakraborty, A. 2020a. Dissipative SymODEN: Encoding Hamiltonian Dynamics with Dissipation and Control into Deep Learning. In *ICLR 2020 Workshop on Integration of Deep Neural Models and Differential Equations*.

Zhong, Y. D.; Dey, B.; and Chakraborty, A. 2020b. Symplectic ODE-Net: Learning Hamiltonian Dynamics with Control. In *8th International Conference on Learning Representations, ICLR 2020, Addis Ababa, Ethiopia, April 26-30, 2020*. OpenReview.net.

Zhong, Y. D.; Dey, B.; and Chakraborty, A. 2021. Benchmarking Energy-Conserving Neural Networks for Learning Dynamics from Data. In *Learning for Dynamics and Control*, 1218–1229. PMLR.

Zhong, Y. D.; and Leonard, N. 2020. Unsupervised learning of lagrangian dynamics from images for prediction and control. *Advances in Neural Information Processing Systems*, 33.

Neural Networks with Physics-Informed Architectures and Constraints for Dynamical Systems Modeling: Supplementary Material

Implementation Details

All numerical experiments were implemented using the python library *Jax* (Bradbury et al. 2018), in order to take advantage of its automatic differentiation and just-in-time compilation features. Project code is publicly available at: <https://github.com/wuwushrek/physics-constrained-nn>.

All experiments were run locally on a desktop computer with an Intel i9-9900 3.1 GHz CPU with 32 GB of RAM and a GeForce RTX 2060, TU106. A complete training run of roughly 10000 gradient iterations, takes approximately 5 to 10 minutes of wall-clock time on the GPU.

Hyperparameters. Table 1 lists the values of the hyperparameters that were used to generate the experimental results.

		Double pendulum	Ant	Fetch	Humanoid	Reacher	UR5E
MLP Construction	Hidden layers	2	2	2	2	2	2
	Nodes per layer	256	512	512	512	256	512
	Activation function	ReLU	ReLU	ReLU	ReLU	ReLU	ReLU
Training Parameters	Optimizer	ADAM	ADAM	ADAM	ADAM	ADAM	ADAM
	Learning rate	$5e-3$	$5e-3$	$1e-3$	$1e-3$	$1e-2$	$1e-2$
	Minibatch size	64	64	64	64	64	64
Constraint Enforcement	Early stopping patience	1000	1000	1000	1000	1000	1000
	Num. points $ \Omega $	10,000	50,000	60,000	120,000	—	—
	Minibatch size $ \Omega _{batch}$	256	128	128	128	—	—
	Initial penalty term μ_0	$1e-3$	$1e-3$	$1e-3$	$1e-3$	—	—
	Penalty multiplier μ_{mult}	1.5	1.5	1.5	1.5	—	—
Other Parameters	Constraint loss tolerance ϵ	$1e-4$	$5e-4$	$1e-3$	$1e-3$	—	—
	Rollout length n_r	5	5	4	4	8	8
	Num. random seeds	3	3	3	3	3	3

Table 1: The hyperparameter values used in the experiments.

Supplementary Double Pendulum Details and Results

Dynamics of Double Pendulum. The full dynamics of the double pendulum are given by (13)-(16).

$$\ddot{\phi}_1 = \frac{g_1(\phi_1, \phi_2, \dot{\phi}_1, \dot{\phi}_2) - \alpha_1(\phi_1, \phi_2)g_2(\phi_1, \phi_2, \dot{\phi}_1, \dot{\phi}_2)}{1 - \alpha_1(\phi_1, \phi_2)\alpha_2(\phi_1, \phi_2)}; \quad \ddot{\phi}_2 = \frac{-\alpha_2(\phi_1, \phi_2)g_1(\phi_1, \phi_2, \dot{\phi}_1, \dot{\phi}_2) + g_2(\phi_1, \phi_2, \dot{\phi}_1, \dot{\phi}_2)}{1 - \alpha_1(\phi_1, \phi_2)\alpha_2(\phi_1, \phi_2)} \quad (13)$$

$$\alpha_1(\phi_1, \phi_2) = \frac{l_1}{l_2} \left(\frac{m_1}{m_1 + m_2} \right) \cos(\phi_1 - \phi_2); \quad \alpha_2(\phi_1, \phi_2) = \frac{l_1}{l_2} \cos(\phi_1 - \phi_2) \quad (14)$$

$$g_1(\phi_1, \phi_2, \dot{\phi}_1, \dot{\phi}_2) = -\frac{l_1}{l_2} \left(\frac{m_2}{m_1 + m_2} \right) \dot{\phi}_2^2 \sin(\phi_1 - \phi_2) - \frac{g}{l_1} \sin(\phi_1) \quad (15)$$

$$g_2(\phi_1, \phi_2, \dot{\phi}_1, \dot{\phi}_2) = \frac{l_1}{l_2} \dot{\phi}_1^2 \sin(\phi_1 - \phi_2) - \frac{g}{l_2} \sin(\phi_2) \quad (16)$$

Where ϕ_1 and ϕ_2 are the angular positions of the two links of the pendulum, m_1 and m_2 denote to the masses at the end of the two links, l_1 and l_2 denote the lengths of the links, and g is the gravity of Earth. For a full derivation of these dynamics, we refer the reader to (Assencio 2014).

Details of the Symmetry Constraints on g_1 and g_2 Used as A-Priori Knowledge (K2). The four equality constraints included as a-priori knowledge are given by equations (17)-(20).

$$g_1(x_{1:2}, x_{3:4}) = -g_1(-x_{1:2}, x_{3:4}), \quad (17)$$

$$g_2(x_{1:2}, x_{3:4}) = -g_2(-x_{1:2}, x_{3:4}), \quad (18)$$

$$g_1(x_{12}, x_{3:4}) = g_1(x_{1:2}, -x_{3:4}), \quad (19)$$

$$g_2(x_{1:2}, x_{3:4}) = g_2(x_{1:2}, -x_{3:4}). \quad (20)$$

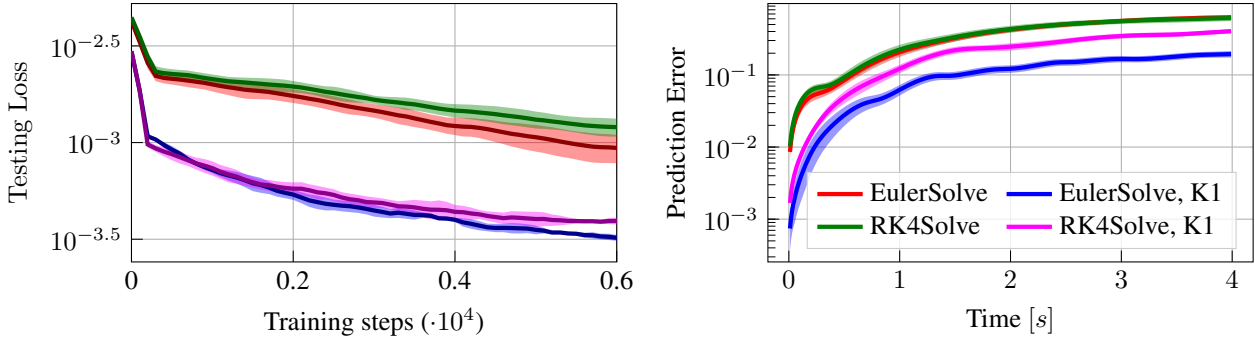


Figure 7: Comparison of the loss function’s evolution when using a first order euler method vs. a fourth-order Runge-Kutta method as the ODE solver. Although RK4 provides the same accuracy as the first order Euler scheme when there is no prior knowledge, it becomes an order of magnitude less accurate than Euler when prior knowledge is incorporated into the model.

Generating the Training and Testing Datasets. In order to generate training data, the above dynamics were integrated using the Dormand-Prince Runge-Kutta ODE integrator (Dormand and Prince 1980) implemented within Jax (Bradbury et al. 2018). The training dataset consists of a single trajectory of 300 datapoints, with a timestep size of $\Delta t = 0.01[s]$. The testing dataset consists of 10 trajectories of each with 300 datapoints each and with the same timestep size. The initial point of each trajectory used for training is sampled from the intervals $\phi_1^{init} \in [-0.5, 0]$, $\phi_2^{init} \in [-0.5, 0]$, $\dot{\phi}_1^{init} \in [-0.3, 0.3]$, and $\dot{\phi}_2^{init} \in [-0.3, 0.3]$. The initial point of each trajectory in the testing dataset is uniformly sampled from the intervals $\phi_1^{init} \in [-0.5, 0.5]$, $\phi_2^{init} \in [-0.5, 0.5]$, $\dot{\phi}_1^{init} \in [-0.6, 0.6]$, and $\dot{\phi}_2^{init} \in [-0.6, 0.6]$. This slight difference in the testing and training datasets helps demonstrate that the incorporation of a-priori knowledge into the model yields better generalization results.

Impact of the Choice of ODE Solver. Recall that the proposed framework requires a *differentiable* ODE solver in order to compute the loss function. The choice of the specific ODE solver used is a hyperparameter of the learning process which influences the accuracy of the model when incorporating a-priori knowledge. We consider two ODE solvers in this paper. The first is the straightforward first-order Euler scheme given by

$$x_{k+1}^\Theta = \text{EulerSolve}(x_k, u_k; F) = x_k + (t_{k+1} - t_k)F(x_k, u_k, G_\Theta(x_k, u_k)), \quad (21)$$

and the second ODE solver is given by a fourth-order Runge-Kutta scheme as follows:

$$k_1 = F(x_k, u_k, G_\Theta), \quad (22)$$

$$k_2 = F(x_k + \frac{1}{2}k_1, u_k, G_\Theta), \quad (23)$$

$$k_3 = F(x_k + \frac{1}{2}k_2, u_k, G_\Theta), \quad (24)$$

$$k_4 = F(x_k + k_3, u_k, G_\Theta), \quad (25)$$

$$x_{k+1}^\Theta = \text{RK4Solve}(x_k, u_k; F(\cdot, \cdot, G_\Theta)) = x_k + \frac{1}{6}(t_{k+1} - t_k)(k_1 + 2k_2 + 2k_3 + k_4) \quad (26)$$

Figure 7 compares the results of using either the fourth-order Runge-Kutta scheme or a first-order Euler scheme when training the model. We observe that, in contrast to what one might expect, training the model using RK4Solve does not result in lower testing loss or prediction error values than when the model is trained using EulerSolve. Instead, the model trained using RK4Solve performs slightly worse than the model trained using EulerSolve. Meanwhile, RK4Solve requires four evaluations of $F(\cdot, \cdot, G_\Theta)$, while EulerSolve requires only one. This demonstrates that the best ODE solver to use in the context of training neural network dynamics models should be evaluated on a case-by-base basis; it may be the case that the more computationally expensive solver results in models that are less accurate.

Additional Experimental Results. Figure 8 gives further comparisons of the errors of the learned double pendulum dynamics models, while Figure 9 illustrates the learned dynamics from a given initial point.

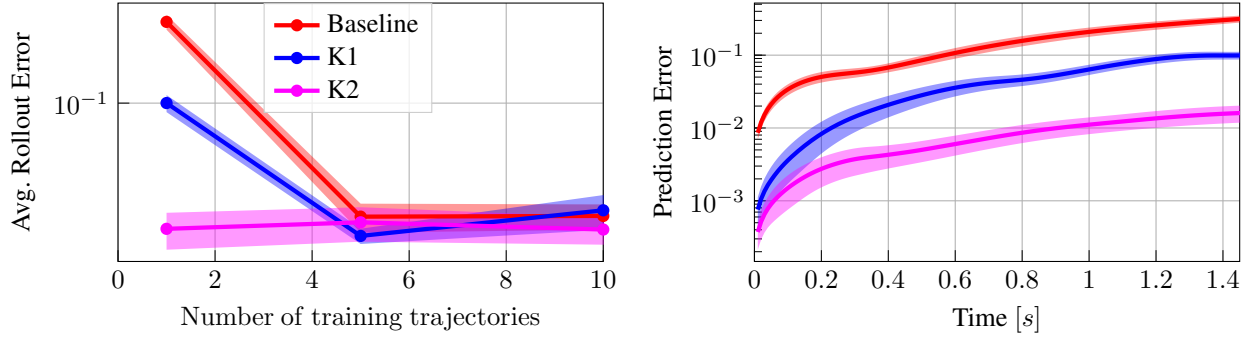


Figure 8: Error comparison of the dynamics models of the double pendulum. The *Avg. Rollout Error* plot shows the average error (calculated over a number of short rollouts) as a function of the number of trajectories included in the training dataset. The *Prediction Error* plot shows the geometric mean of the model prediction error (calculated over several short rollouts) as a function of time. All plots are generated using models whose training has converged.

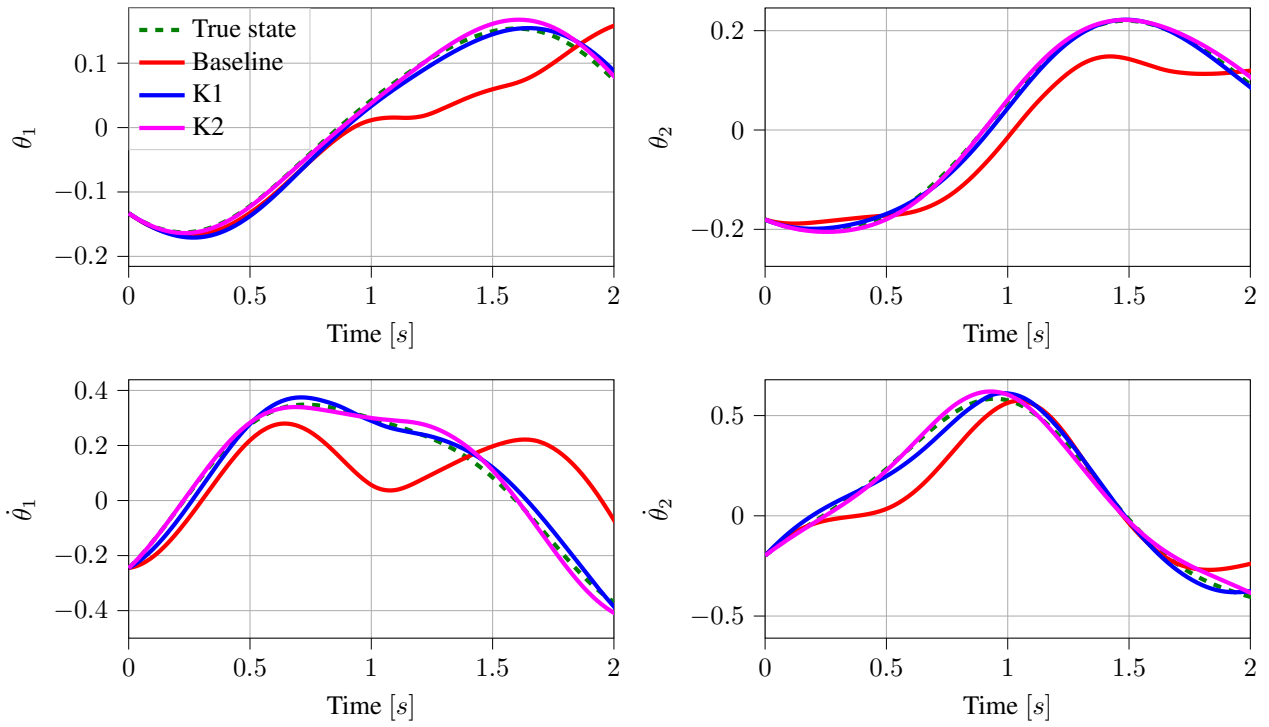


Figure 9: Estimated dynamics of the double pendulum system.

Supplementary Robotics Experiments Details and Results

Complete Brax Dynamics. We recall that the dynamics of multi-body rigid systems are in general given by

$$\ddot{q} = M(q)^{-1}[C(q, \dot{q}) + \tau(q, \dot{q}, u) + J(q)\mathcal{F}(q, \dot{q}, u)], \quad (27)$$

where q represents the position or angle of the bodies, and \dot{q} represents the velocity or rotational velocities of the bodies.

However, Brax's implementation of the dynamics is slightly different from those given above. In fact, angular values q are instead represented by quaternions. Specifically, the system's state is given by $q = [\text{pos}, \text{quat}]$ and $\dot{q} = [v, \omega]$, where pos is the position, quat is the quaternion representation of the angular positions, v is the velocity, and ω is the rotation velocity. Thus, the actual full dynamics of the system are given by:

$$\text{p}\dot{\text{os}} = v; \quad \text{quat} = \frac{1}{2}[0; \omega] \cdot \text{quat}; \quad \ddot{q} = M(q)^{-1}[C(q, \dot{q}) + \tau(q, \dot{q}, u) + J(q)\mathcal{F}(q, \dot{q}, u)], \quad (28)$$

where \cdot denotes the product between two quaternion values.

In this paper, (K1) assumes the a-priori knowledge that $\text{p}\dot{\text{os}} = v$; $\text{quat} = \frac{1}{2}\omega \cdot \text{quat}$ is given.

Environment Details. As each environment in Brax is essentially composed of multiple bodies, some bodies in the environments might be inactive. That is, their states do not evolve in time. For example, the ground in each environment is considered to be inactive. In these settings, we reduce the number of states present in q and \dot{q} by eliminating these variables and learning the dynamics of the active states only.

	Ant	Fetch	Humanoid	Reacher	UR5E
Number of control inputs	8	10	17	2	6
Number of active states	117	143	143	12	78
Total number of states	130	169	156	52	104

Table 2: The number of states and control variables in each brax environment.

Additional Experimental Results. We provide the experimental results for all of the robotics environments below. We note that the *Ant*, *Fetch*, and *Humanoid* experiments feature contact forces, while the *Reacher* and *UR5E Arm* experiments do not. We accordingly only include the results of the (K3) and (K4) experiments (which incorporate a-priori knowledge pertaining to the contact forces) for the former three environments.

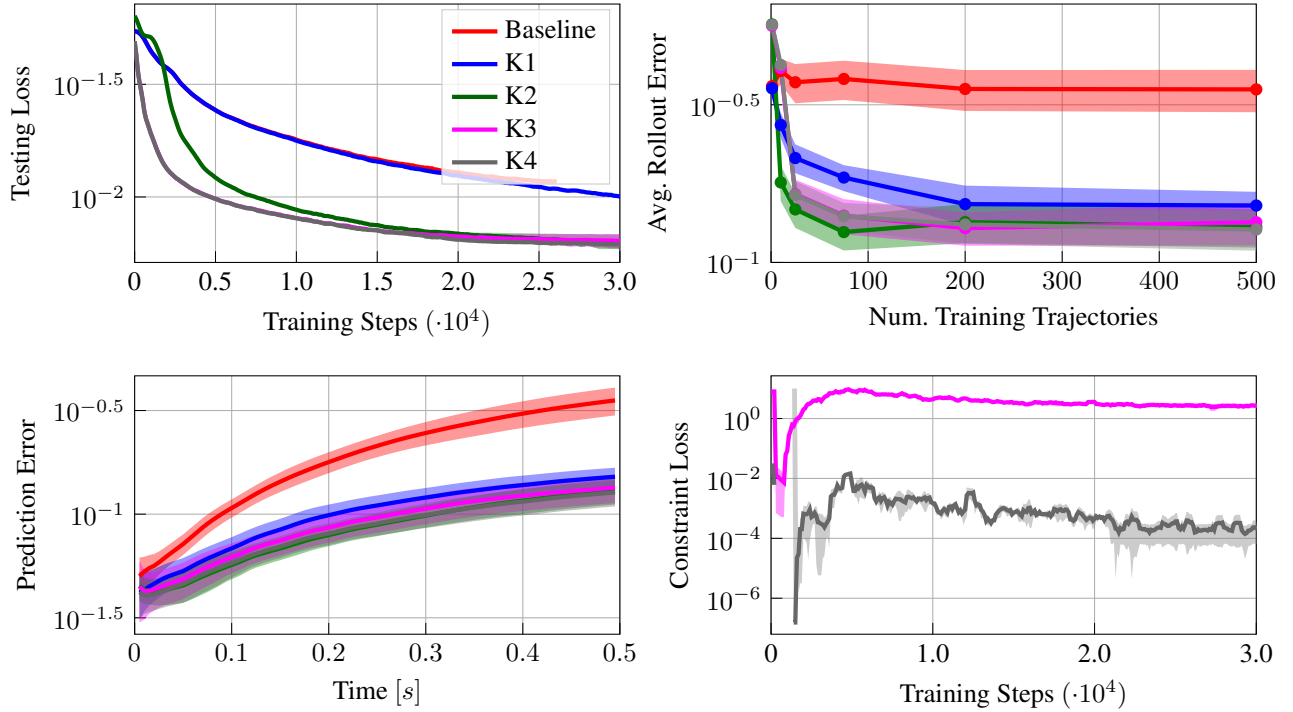


Figure 10: Supplementary results for the *Ant* experiments. We note that in the *Testing Loss* plot, the Baseline curve is almost entirely covered by that of *K1*.

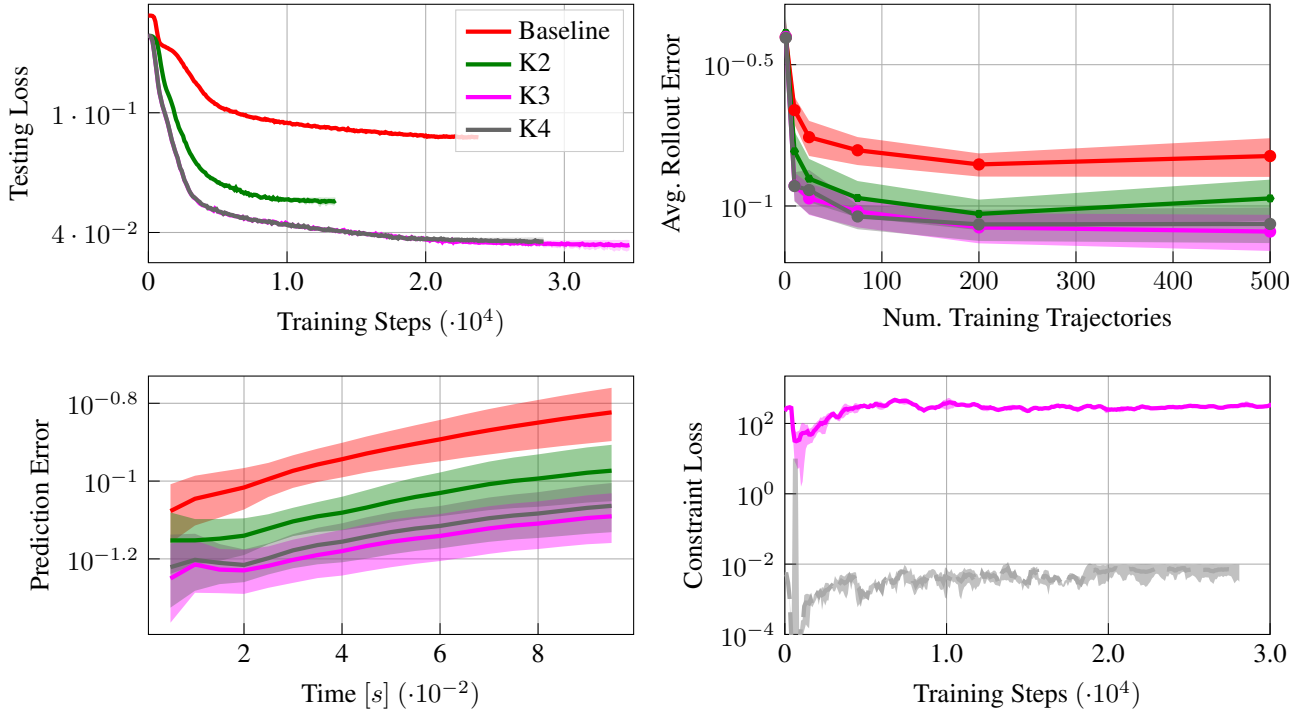


Figure 11: Supplementary results for the *Fetch* experiments.

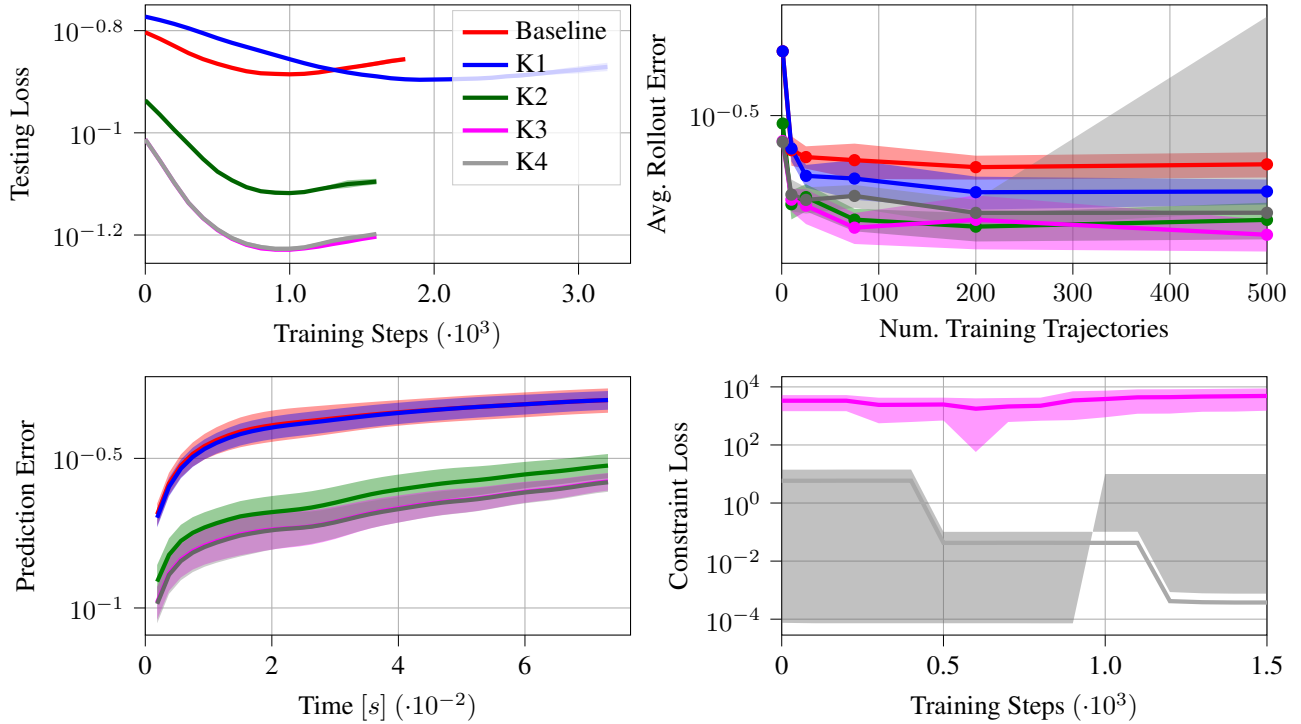


Figure 12: Supplementary results for the *Humanoid* experiments.

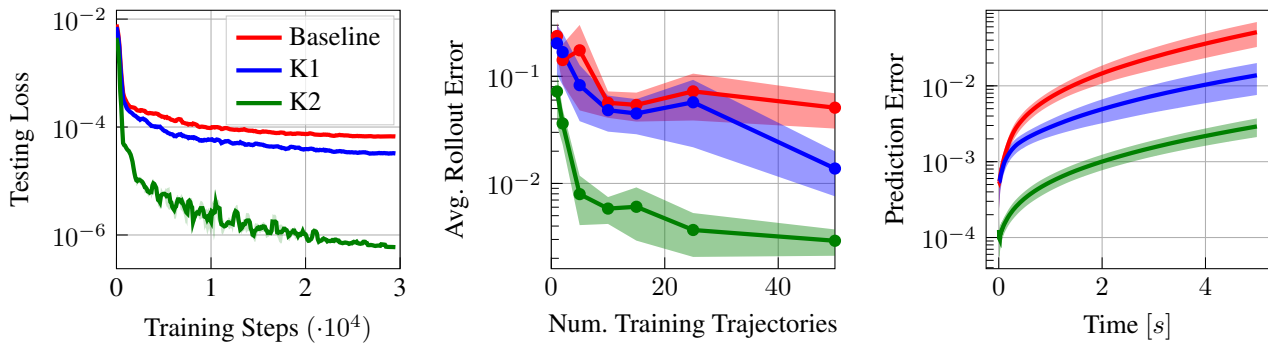


Figure 13: Supplementary results for the *Reacher* experiments.

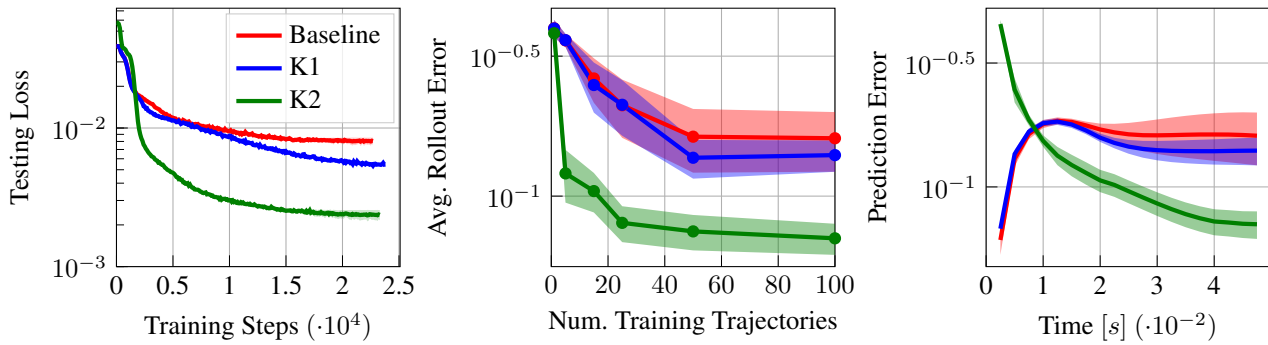


Figure 14: Supplementary results for the *UR5E* experiments.